JTTEE5 16:229–237
DOI: 10.1007/s11666-007-9031-x
1059-9630/$19.00 © ASM International

In Flight Properties of W Particles in an Ar-H_2 Plasma

Ondřej Kovářík, Xiaobao Fan, and Maher Boulos

(Submitted May 10, 2006; in revised form September 4, 2006)

An in-flight properties measurement performed on W particles, injected into thermal plasma generated by an inductively coupled RF plasma torch, is presented. The measured surface properties of the particles along the centerline of the plasma plume are expressed by means of temperature and velocity maps, within the domain formed by individual particle's diameters and their distances from the torch exit. The influence of some of the processing parameters (plate power, carrier gas flow rate, spray chamber pressure) on particle properties is discussed for both individual particles and the resultant integral spray plume characteristics. The results so obtained appear to confirm the suitability of the RF plasma process for the deposition/production of W coatings/deposits.

Keywords in-flight properties, RF-induction plasma, tungsten

1. Introduction

During the thermal spray process, particulate feedstock material is heated and accelerated by the hot plasma stream and the spray plume is formed by the hot feedstock material particles. The spray plume is projected onto a suitable substrate, thereby forming the thermal spray deposit. In order to obtain deposits of the desired quality, the particles must impinge on the substrate at certain optimal values of velocity, temperature, and melting status. The in-flight particle's properties provide a useful means for the characterization of the thermal spray process, this being much more important than the actual values of the process's individual parameters. Clearly, similar spray plume properties at the point of impact should lead to similar deposit properties, regardless of the spray conditions or even the actual spray technologies used (assuming similar substrate states are employed). This paper introduces a novel graphical representation of in-flight particle data, which enables integrated description of velocity and temperature development of individual particles of the spray plume.

Numerous studies of in-flight particle behavior during plasma forming were conducted up-to date, both numerically and experimentally. Numerical simulations consist of modeling both the plasma properties and either coupled or uncoupled plasma-particle heat and momentum transfer. The computations of properties of RF inductively coupled thermal plasma in local thermodynamical equilibrium (LTE) (Ref 1) or in non-LTE conditions (Ref 2, 3), using standard or extended (Ref 4) field models, have been published. A comparison of the simulation data with the experimental measurement (enthalpy probe) is available in (Ref 5). Particle/plasma interaction models have been developed from uncoupled discrete/continuous phase models of the individual particles behavior (Ref 6, 7) to models of coupled plasma-particle interactions using several hundred particles of different sizes and startup velocities (Ref 8-11).

Experimental studies are based mostly on two-color pyrometry combined with the time of flight method (Ref 12-14), the laser anemometry methods, or on image analysis of high-speed cameras images (Ref 15). These methods offer simultaneous measurements of a single particle for its diameter, velocity, and temperature, and are widely available due to the successful commercial realization of the method in the DPV-2000 particle sensor instrument. Comparison of measurement and model are presented i.e., in (Ref 16, 17).

The measured or computed data are presented either in forms of particle property histograms (Ref 12), individual particle momentum and thermal histories for a few particle diameters (Ref 7, 10, 11, 17, 18), or as a time development of mean values or other statistics of T and v (Ref 19, 20). Some authors have reported correlations between particle diameter d_p and particle temperature T_p or velocity v_p (Ref 17, 18). Such a correlation is not reflected in particle properties histograms, thus particle history with respect of d_p appear more appropriate for the description of spray plume.

Particle history (with respect to distance z_p from torch exit) for all particle diameters can be described by a z_p/d_p map. In order to construct the z_p/d_p map, particles are grouped into classes of similar particle diameter d_p and measurement position z_p. The stochastic nature of the spray plume leads to random differences between the particle temperature T_p and the velocity v_p, for particles of

Ondřej Kovářík and **Maher Boulos,** Department of Chemical Engineering, University of Sherbrooke, Sherbrooke, QC, Canada; **Xiaobao Fan** and **Maher Boulos,** Tekna Plasma Systems Inc., Sherbrooke, QC, Canada. Contact e-mail: kovon@seznam.cz.

the same class (even for the same d_p and z_p). Thus, statistical description (mean value, median, 10% quantile, etc.) must be used. The median values of T_{50} and v_{50} were chosen for the exercise described.

The z_p/d_p map provides complex set of particle property information; however for simple scalar description of spray parameters effect, *integral spray plume* properties are sometimes used throughout this paper. Volumetric medians, T_{V50}, v_{V50}, or d_{V50} can be computed for different z_p. The volumetric median is a temperature (or velocity) such that some 50% by volume of the measured particles are warmer (or faster, or bigger) than the volumetric median value.

This paper summarizes the axial distribution of in-flight particle properties, of particles with trajectories close to the plasma plume centerline, as obtained during a case study of W deposition by RF-plasma. The data are presented for various sets of process parameters, viz., applied plate power P, carrier gas flowrate q_c, and chamber pressure p. Variations in the spray plume data along the radial axis were not studied in this instance.

2. Experimental

Commercial tungsten powder, grade Amperite Am 140.2, of grain size $-90+45$ μm, was used as the spray feedstock material (see Fig. 1a).

Spraying was performed using the Tekna PL-50 induction plasma torch (Tekna Plasma Systems Inc., Sherbrooke, Quebec, Canada). The torch has a 50 mm ID and contains a seven-turn induction coil. The RF frequency is 300 kHz.

The powder was injected into the plasma at the axial position, corresponding to the lowest turn of the induction coil, in order to avoid powder recirculation within the plasma. The powder feeder, Tekna PF-400, was used with He as the carrier gas. A vacuum chamber, equipped with an automatic pressure regulator, was maintained at constant pressure throughout the whole experimental period.

Process Parameters: Two levels of each process parameter were used in order to conduct a full factorial experiment of three factors: the plate power P (60, 80 kW), carrier gas flow rate q_c (6.3, 9.5 slpm), and chamber pressure p (300, 400 torr). The factor levels were selected based on the observations of previous works (Ref 20-23). Ar-H_2 plasma was used, with a central Ar flow rate of 30 slpm, sheath Ar at 90 slpm, and sheath H_2 at 15 slpm. The feed rate for the W powder was fixed at 40 g/min, to provide sufficient throughput for potential industrial applications.

Particle surface temperature T_p, velocity v_p, and diameter d_p of individual particles were measured by the DPV-2000 particle sensor (Tecnar, St. Bruno, QC, Canada). The position of the sensor was at a distance z_p from the torch exit nozzle and the centerline of the spray plume was observed. Distances $z_p = \{120, 140, 160, 200, 230, 260, 290, 320\}$ mm were employed. Due to the high emissivity and temperature of W spray particles, an aperture collar was developed in order to reduce the infrared radiation entering the DPV-2000 sensor. Ar gas was passed through the collar to shield the sensor window from contamination. The sensor, and its optical fiber connection, was contained in a water-cooled enclosure, fitted with quartz window. An overview of the sensor-collar assembly is shown in Fig. 2. The temperature measurement is based on Wien approximation of Planck law (Ref 12, 24):

$$T(K) = \frac{A}{\ln\left(\frac{U_{D1}}{U_{D2}}\right) + B}$$

Here U_{D1} and U_{D2} are signals from the infrared detectors. The constants A and B were calibrated up to 2400 °C using W filament. Above 2400 °C, the validity of the calibration is only assumed. The diameter measurement is proportional to square root of total energy emitted by a particle of known temperature (Ref 24).

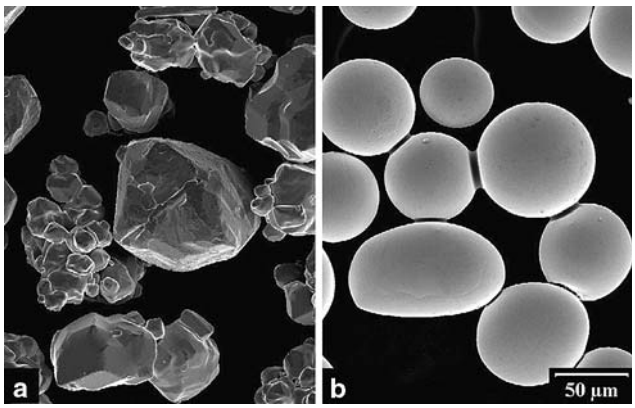

Fig. 1 SEM micrographs of the 'as-received' powder (a) and powder spheroidized during the spray process (b)

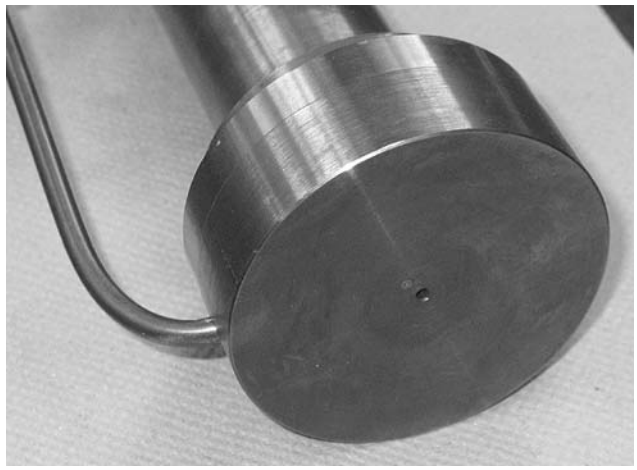

Fig. 2 The aperture collar shielding the DPV-2000 sensor window

$$d = C\sqrt{\frac{E}{T_p^4}}$$

The constant C has to be calibrated against a known sample. Based on previous works (Ref 19) it was expected that in the investigated z_p range, most of the particles will be already spheroidized, and thus the particle size distribution will be different to that of as-received powder. Thus the volumetric median diameter of particles collected in a special insulated container (Ref 19) was used for calibration. The process parameters for the calibration run were $P = 60$ kW, $p = 400$ torr, $q_c = 6.3$ slpm, other parameters as described above. The particle collector was placed at $z_p = 170$ mm distance from the torch exit. As it will be shown later, all the particle temperatures were well inferior to the boiling point of W thus no particle evaporation was considered. Image analysis of collected powder indicates $d_{V50} = 60$ μm.

For the operating principle of the DPV-2000 instrument, please refer to (Ref 24). The spray plume was subject to analysis for 60 s at each chosen distance z_p, measured from the torch exit. The actual measurement period started ~30-40 s after powder feeding had commenced, in order to obtain steady-state conditions inside the reactor. Each collection of measurement data consisted of approximately 400-1600 triplets, d_p, T_p, v_p, corresponding to individual powder particle observations. The data were further processed in a Matlab routine to obtain the z_p/d_p maps.

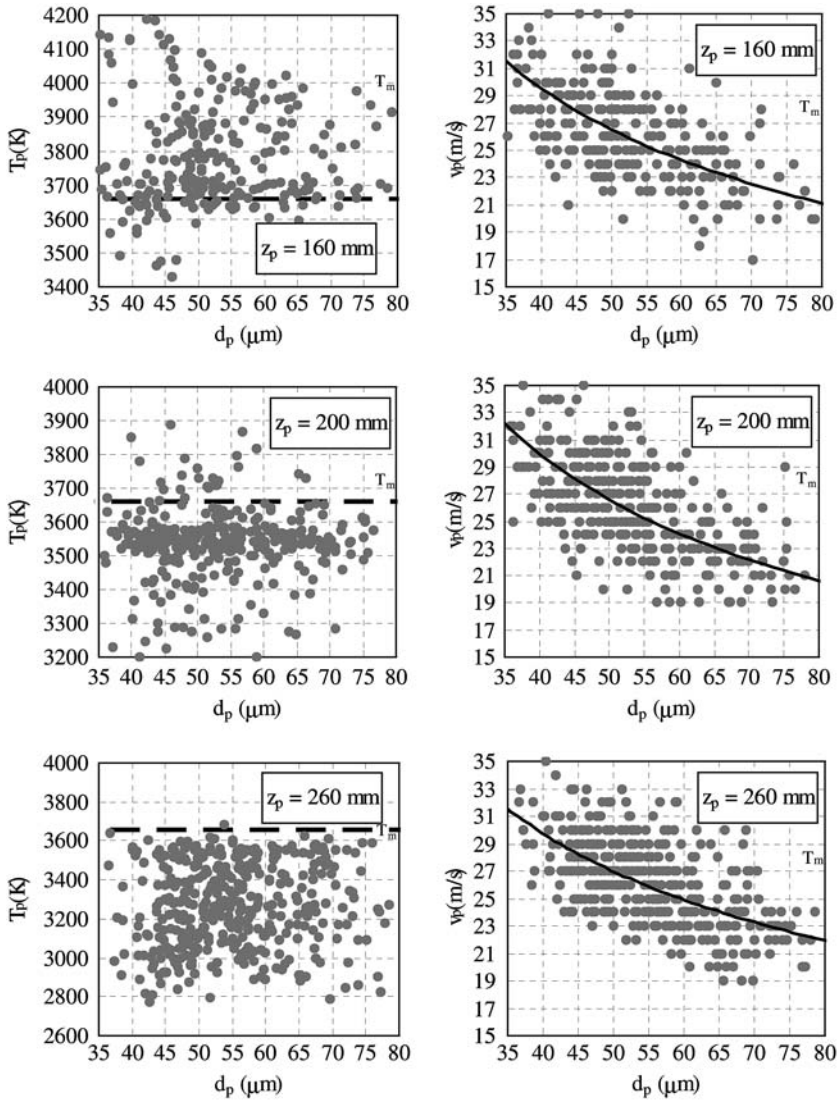

Fig. 3 The temperature T_p and velocity v_p of particles for $P = 60$ kW, $p = 400$ torr, $q_c = 6.3$ slpm, and $z_p = 160$, 200, 260 mm. Note the accumulation of T_p between 3450 and 3650 K due to phase transformation at 160 mm. The velocity data is approximated by formula $v_p = Ad_p$

3. Results and Discussion

3.1 Individual Particle Properties

Experimental data collected by the DPV-2000 instrument are presented in Fig. 3 for spray conditions $P = 60$ kW, $p = 400$ torr, $q_c = 6.3$ slpm. The T_p/d_p and v_p/d_p charts are given for three selected z_p distances to represent different cooling stages of the particles. The first set of charts ($z_p = 160$ mm) describes the cooling of particles in liquid state, the second set ($z_p = 200$ mm) describes the phase transformation, and the third set ($z_p = 260$ mm) cooling in the solid state. The experimentally measured temperature of the phase transformation area in Fig. 3 appears to be between 3450 and 3650 K (see Fig. 3, $z_p = 200$ mm), which agrees well to the melting point of W (3663 K). This agreement justifies the temperature measurement method used. The somehow (about 4%) lower measured particle temperature was not explained yet. One possible cause is the undercooling of W particles. However, due to measured fast cooling rates and expected very fast recalescence rates (see i.e., model (Ref 25)), the probability to detect a particle in undercooled state is very low. Moreover, the low standard deviation of particle temperature during solidification indicates, that undercooling and following recalescence are not detected during the measurements. In the following discussion, any particle with a measured surface temperature between 3450 and 3650 K is considered to undergo phase transformation. Below 3450 K, the particles are considered to be completely solid.

The velocity of the particle is controlled by the propulsion force of the carrier and plasma gases and by the gravity force. Generally, a steady increase in particle velocity was observed with increasing z_p (see Fig. 4-7). Also a strong correlation between particle diameter and velocity was observed (see Fig. 3). The velocity of the particles follows the formula:

$$v_p = A d_p^n$$

in which the exponent n was nearly constant for all observed conditions ($n \sim -0.5$). The measured velocities are similar to that of Alumina particles measured in (Ref 12) with the same torch, but generator frequency of 3 MHz.

It should also be mentioned, that due to the different thermal histories of the particles of similar (±5 μm) diameter, and the measurement uncertainty, the typical standard deviation of the particle temperature T_p, is about 200-250 °C and it drops significantly (~100 °C) during phase transformations. For the velocity, the standard deviation is about 4 m/s.

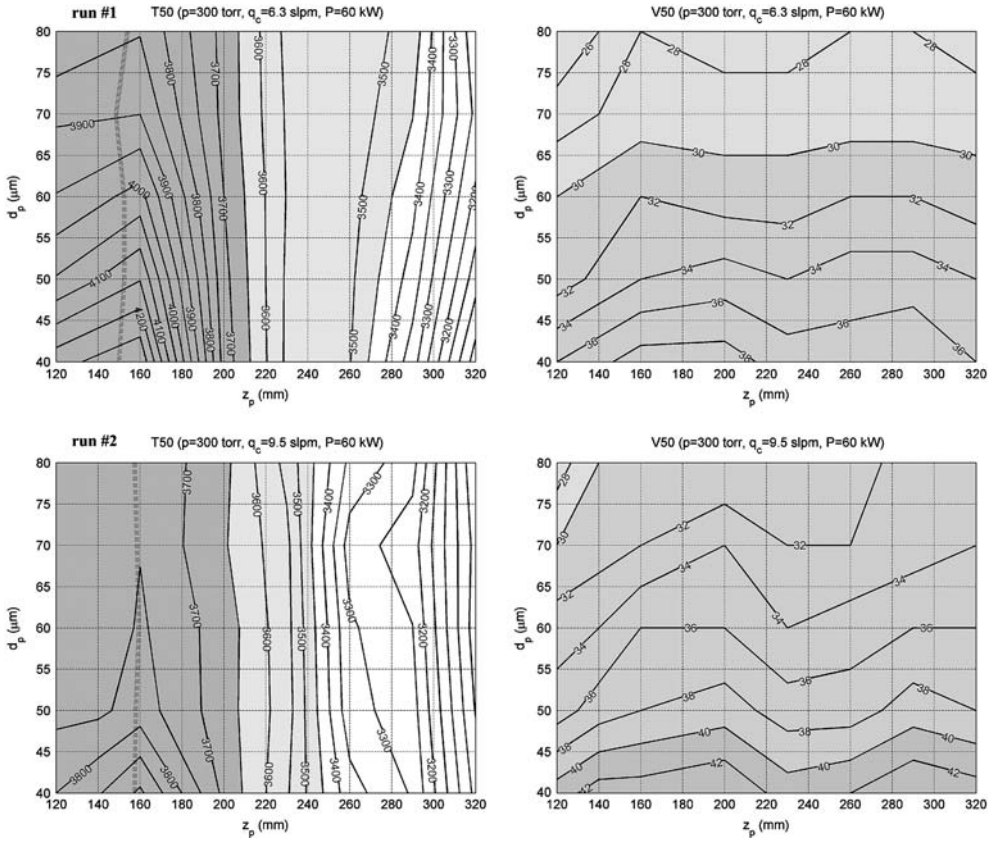

Fig. 4 z_p/d_p maps for p = 300 torr, P = 60 kW. Left: of median particle temperature T50 (isocontours in K). The white areas correspond to solid particles, light gray to particles undertaking phase transformation (phase transformation area), and dark gray to liquid particles. The maximum temperature line is included. Right: z_p/d_p maps of median particle velocity v50 (isocontours in m/s)

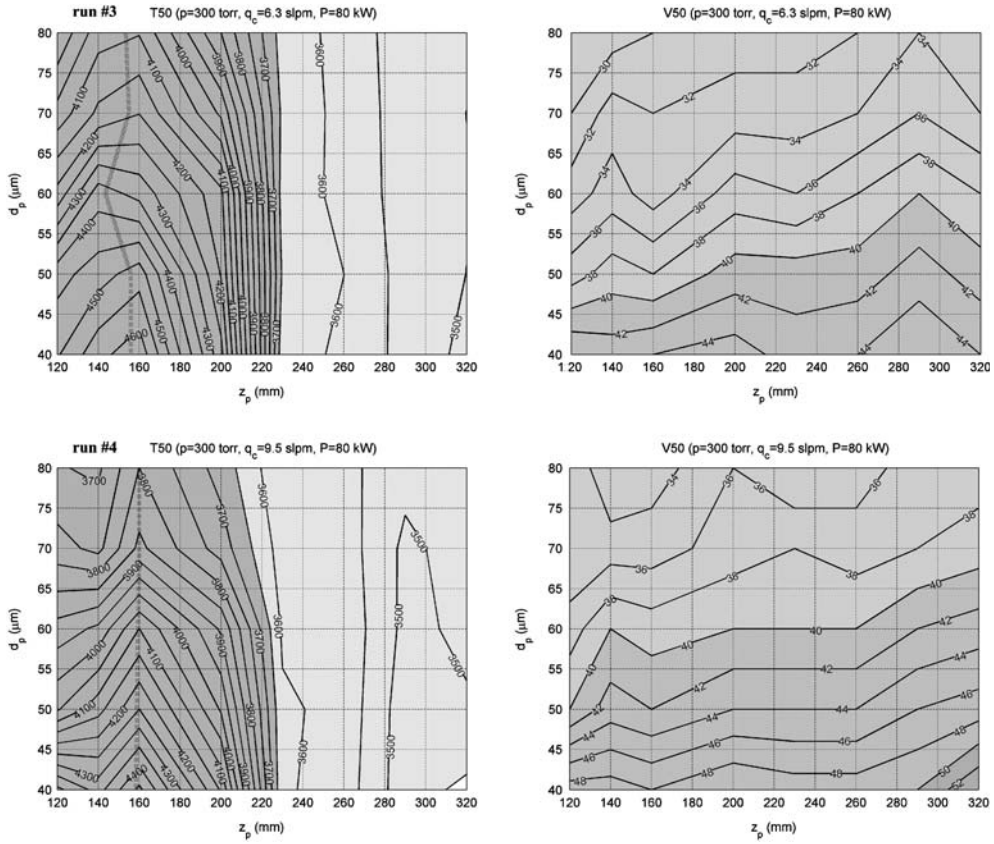

Fig. 5 z_p/d_p maps as in Fig. 4, but for $p = 300$ torr, $P = 80$ kW

The processed individual particle data form z_p/d_p temperature and velocity maps for each combination of investigated process parameters (process parameters are summarized in Table 1). The z_p/d_p maps are set out in Fig. 4-7 following the order of Table 1. From the individual maps, median particle temperature T_{50} and velocity v_{50}, as a function of z_p, can be obtained by traversing the map in the z_p sense (for fixed d_p), whereas the influence of d_p on T_{50} and v_{50} is obtained by traversing in the $d_p$sense (for fixed z_p).

For temperature maps, the influence of z_p is much stronger than the influence of d_p, thus the isolines are mostly vertical. Opposite situation takes place for velocity maps, where the governing factor is d_p, which is in agreement with the majority of numerical studies [see i.e., (Ref 16-19)].

The results indicate, that the used range of z_p covers mostly cooling parts of particle trajectories. It is straightforward, that this part of particle trajectory directly influences the properties of final deposit. The typical features of the z_p/d_p temperature maps of the investigated area are as follows.

The *maximum temperature line* is formed by a set of points where particles of given size reach their maximum temperature. As may be expected from the particle surface to volume ratio, the smaller particles will be heated significantly faster and will reach higher temperatures sooner than the larger particles (similar results reported in (Ref 6, 7, 17, 18), etc.). At the same time, larger particles, with their higher thermal inertias, should reach their maximum temperature values at higher z_p than smaller particles and cool slower. This should cause the maximum temperature line to have a slope of a couple of degrees clockwise from the d_p axis. However this phenomenon was not observed in the investigated cases, indicating that particles reach their maximum temperature at the same z_p regardless of particle diameter d_p. This state is caused by the v_p/d_p relation and is favorable for W deposition. In the area above the melting point, close to the maximum temperature line, the influence of d_p on T_{50} is significant. In this area, the theoretical studies report significantly different temperatures for different particle diameters (i.e. (Ref 10, 11, 18)). On the other hand after solidification, the influence of d_p was significantly weaker in most cases with the exception of $p = 400$ torr and $P = 80$ kW.

When phase changes take place, the particle surface temperature remains at the melting point (the undercooling and recalescence phase is considered short and is neglected based on model in (Ref 25)) until the phase transformation is finished (this assumption is based on high thermal conductivity of the feedstock material and the low particle velocity). Thus, a *phase transformation area*, where the majority of particles stay close to the melting point, is created. It is interesting to note that the different size and position of the phase transformation area was observed for the different applied power levels.

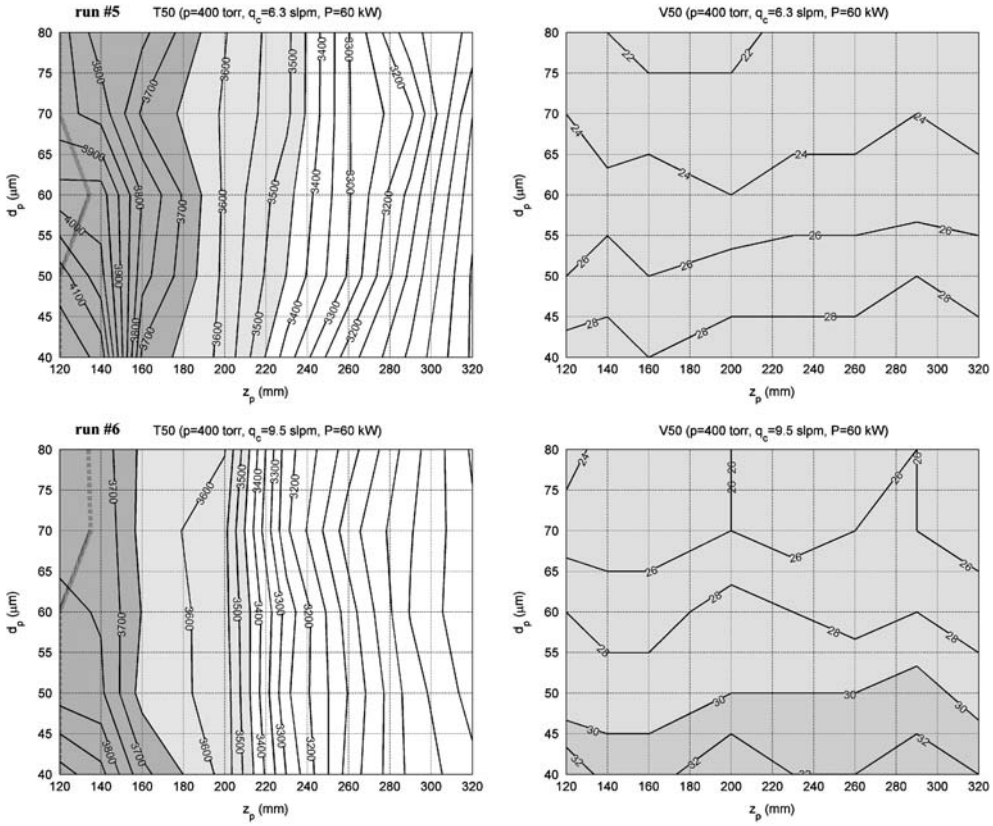

Fig. 6 z_p/d_p maps as in Fig. 4, but for $p = 400$ torr, $P = 60$ kW

However, at the same time, the position of the maximum temperature line was very similar for both power levels.

Some noise and ''artifacts'' (in the form of jagged contour lines) can be observed on the presented z_p/d_p maps, especially in the large particle areas. The most significant cause of these defects is the limited number of detected and measured particles belonging into certain classes of map. However, increased spraying times (and thus the number of detected particles for all classes) would require increased amounts of expensive feedstock material.

3.2 Integral Particle Properties and Factorial Analysis

The z_p/d_p maps, as presented in Fig. 4-7, clearly illustrate the influence of process parameters on the spray plume. In order to provide a statistical description of this influence, a factorial analysis (Ref 26) was performed. The volumetric median temperature T_{V50} and velocity v_{V50} evaluated at the position of maximum temperature line were chosen as responses of the factorial analysis. In the following text T_{V50} and v_{V50} are always linearly interpolated at measurement distances closest to the maximum temperature line. The position z_m of maximum temperature line was not included in the analysis as the values of z_m are very approximate. The integral particle properties T_{V50} and v_{V50} correspond to properties of particle with $d_p = 60$ μm. The positions of maximum temperature line, values of response variables and levels of factors are summarized in Table 1. The influence of sheath H_2 flow rate is not included in the factorial experiment.

The data in Table 1 were approximated by the least square method as:

$$T_{V50,u} = b_o^T + \sum_{i=1\ldots3} b_i^T X_{i,u} + \sum_{i=1\ldots3} \sum_{j=i+1\ldots3} b_{i,j}^T X_{i,u} X_{j,u}$$

$$v_{V50,u} = b_o^v + \sum_{i=1\ldots3} b_i^v X_{i,u} + \sum_{i=1\ldots3} \sum_{j=i+1\ldots3} b_{i,j}^v X_{i,u} X_{j,u}$$

in which u is the run number from Table 1, ${b_{i,j}}^T$ and ${b_{i,j}}^v$ are regression coefficients for T_{V50} and v_{V50} respectively, $X_{i,u}$ is the value of ith factor for run u. The regression was performed for coded factor levels (−1,1) of $X_{i,u}$ and obtained coefficients are in Table 2. The coefficients ${b_{123}}^T$ and ${b_{123}}^v$ are negligible (see Table 2) compared to other regression coefficients, thus insignificant effect of 3-way interaction of P, q_c, and p is assumed. The significance of other coefficients is assessed by comparing the ratios of $\frac{b_1^v}{b_{123}^v}, \frac{b_2^v}{b_{123}^v}, \ldots, \frac{b_{23}^v}{b_{123}^v}$ and $\frac{b_1^T}{b_{123}^T}, \frac{b_2^T}{b_{123}^T}, \ldots, \frac{b_{23}^T}{b_{123}^T}$ to the $t_{0.95,1}$ value (student distribution with 1 degree of freedom at significance level 0.95). All factors with coefficients resulting in ratios smaller than $t_{0.95,1}$ are assumed insignificant (Table 2).

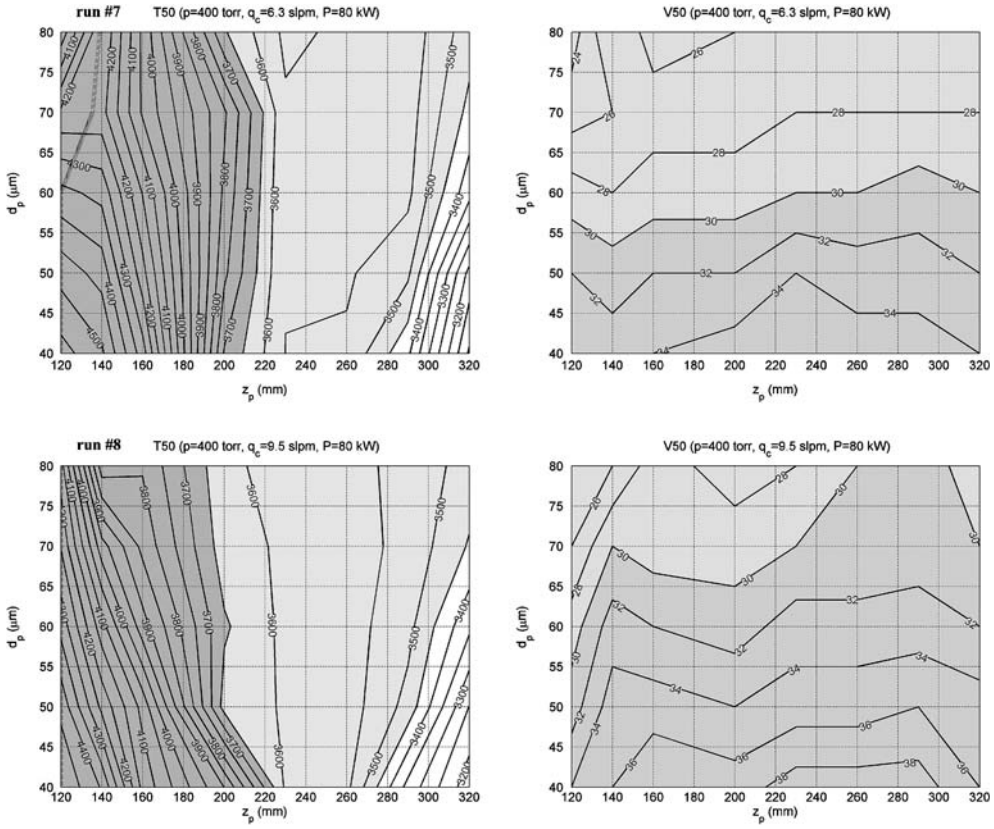

Fig. 7 z_p/d_p maps as in Fig. 4, but for $p = 400$ torr, $P = 80$ kW

Table 1 The influence of integral spray plume properties on process parameters

							η_s (b)	
Run	**$p(X_1)$ (c), torr**	**$P(X_2)$, kW**	**$q_c(X_3)$, slpm**	**z_p (a), mm**	**v_{V50}, m/s**	**T_{V50},K**	**110 mm, %**	**170 mm, %**
#1	300(−1)	60(−1)	6.3(−1)	150	31	4003	84.00	90.00
#2	300	60	9.5(1)	160	35	3756	66.00	80.00
#3	300	80(1)	6.3	150	34	4340	···	···
#4	300	80	9.5	160	38	4068	···	···
#5	400(1)	60	6.3	120	25	3979	94.00	91.00
#6	400	60	9.5	120	26	3744	84.00	88.00
#6	400	80	6.3	120	29	4365	···	···
#8	400	80	9.5	120	29	4124	···	···

(a) Position of maximum temperature line. (b) See (Ref 12). (c) Number in brackets is coded level for factorial analysis, X_1, X_2, X_3 are factors.

Taking only significant coefficients the regression functions for p in torr, q_c in slpm and P in kW, become:

$$v_{V50} = 0.0139\ p + 0.1625\ P + 4.531\ q_c - 0.01094\ p \cdot\ q_c + 9 \quad \text{(Eq 1)}$$

$$T_{V50} = 17.69\ P - 77.73\ q_c + 3423 \quad \text{(Eq 2)}$$

The corresponding regressions in coded factor levels (−1,1) are:

$$v_{V50} = -3.63\ p + 1.63\ P + 1.13\ q_c - 0.88\ p \cdot q_c + 30.9 \quad \text{(Eq 3)}$$

$$T_{V50} = 176.8\ P - 124.3\ q_c + 4047 \quad \text{(Eq 4)}$$

Based on formulas 3 and 4, the effects of different process parameters can be discussed:

Plate power: Increasing the plate power, P from 60 to 80 kW, leads to higher specific enthalpies and larger dis-

Table 2 The coefficients of regression equation for T_{V50} and v_{V50}

Factor		v_{V50}, m/s		T_{V50}, K	
	b_0	30.9		4047	
Principal effects	I	b_i^v	b_i^v/b_{123}	b_i^T	b_i^T/b_{123}
p	1	−3.63	**29.00**	5.63	2.37
P	2	1.63	**−13.00**	176.88	**74.47**
q_c	3	1.13	**−9.00**	−124.38	**−52.37**
Interactions	ij	b_{ij}^v	b_{ij}^v/b_{123}	b_{ij}^T	b_{ij}^T/b_{123}
Pp	12	0.13	−1.00	14.63	6.16
$p\ q_c$	13	−0.88	**7.00**	5.38	2.26
Pq_c	23	−0.13	1.00	−3.88	−1.63
$P\ p\ q_c$	b_{123}	−0.13	1.00	2.38	1.00

charge volumes of the plasma, both effects leading towards higher heat transfers from the plasma to the particles. The result of increasing P is higher particle temperatures and velocities. The increase in velocity v_{V50}, at the maximum temperature line, is about 3 m/s. The temperature T_{V50}, at the maximum temperature line increases by ~350 K.

Carrier gas flow rate: The increase of carrier gas flow rate from 6.3 to 9.5 slpm increases particle to plasma injection velocity, cools the central region of the plasma discharge and, at the same time, increases the plasma gas velocity in the center of the discharge (an in-depth study of this phenomenon is presented in (Ref 5) and further experimental evidence given in (Ref 27)). The effect is further amplified by the fact that most of the particle trajectory is inside the volume influenced by the carrier gas. The resulting reductions in the heat transfer to particles cause the decrease particle temperature T_{V50} by ~250 K. The effect on particle velocity v_{V50} is coupled with chamber pressure. Particle velocity v_{V50} increased by ~4 m/s for $p = 300$ torr, for $p = 400$ torr, the influence was negligible (~0.5 m/s). A simple explanation is that at higher chamber pressure the carrier gas balances its velocity with the plasma gas faster and so the particle velocity is more controlled by the plasma gas velocity.

Chamber pressure: Increasing the chamber pressure p from 300 to 400 torr leads to decreased plasma volumes and plasma gas velocities. As a result of the combined action, the maximum temperature line is always at lower distance z_m from the torch nozzle. The effect on particle velocity v_{V50} is coupled with carrier gas flow rate q_c particle velocity as discussed above. The value of v_{V50} decreased by ~5.5 m/s at $q_c = 6.3$ slpm and by ~9 m/s for $q_c = 9.6$ slpm regardless the plate power P. The value of T_{V50} was not significantly influenced by chamber pressure. These results obtained for generator frequency of 300 kHz are in contrast with previous results for 3 MHz (Ref 12, 22). For 3 MHz, the mean particle temperature is reaching maximum at lower z_m when increasing pressure. At the same time, the mean temperature at z_m is decreasing.

Particle spheroidization: Particle spheroidization efficiency η_s is defined as the ratio of spheroidized particles to the total number particles in collected sample. The spheroidization efficiency was measured for $z_p = 110$ and 170 mm, $p = 300$ and 400 torr and $P = 60$ kW in previous experiments (Ref 20). The particles were collected at the centerline of the plasma plume, through a aperture of 7 mm diameter. For most cases, the particles were collected after the maximum temperature line and after cooling in liquid phase. Thus no effect of particle size on particle spheroidization was detected. The spheroidization ratio was $\eta_s \sim 80$-90% (see Table 1). The only exception is run #2 with a lower value of $\eta_s = 66\%$ for $z_p = 110$ mm. Indeed the z_p/d_p map in Fig. 6, indicates, that the particles collected at $z_p = 110$ mm were probably collected during melting phase. For the same process conditions, but for $z_p = 170$ mm the particles were collected in liquid cooling phase after passing the maximum temperature line and η_s increased to 81%.

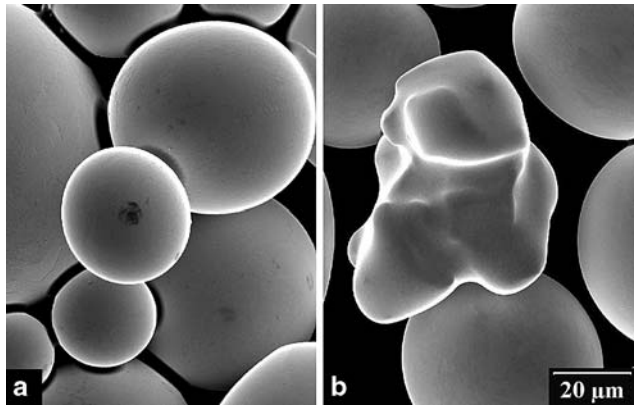

Fig. 8 Plasma-treated particles: (a) well-spheroidized particle and (b) nonspherical particle

An interesting phenomena, commonly observed for refractory metals is that the nonspherical particles are often smaller than already spheroidized particles (see Fig. 8 and (Ref 28)). The possible explanation is the effect of turbulence on particle trajectory as described in (Ref 8). Small particles with low inertia are easily deflected from the spray plume central line and their trajectory passes through turbulent low temperature regions. Thus limited heat is transferred to the particles and incomplete melting occurs.

4. Conclusion

The characterization of the centerline of the spray plume was performed for some eight sets of processing parameters. The data obtained during the spray plume characterization tests included: particle velocities, temperatures, particle size histograms, T_p/d_p plots, v_p/d_p plots, and z_p/d_p maps; these were all subsequently organized in a computer database. Thus, the experimental results so obtained can be used to make a selection of the most suitable spray parameters for the plasma spray deposition of W.

The influence of varying levels of plate power, carrier gas flow rate and chamber pressure on integral properties of the spray plume at position with maximum particle

temperature were all investigated in a full-factorial experiment. It was found that

(i) The volumetric median particle temperature was influenced by plate power and carrier gas flow rate.

(ii) Volumetric median particle velocity was influenced by plate power, carrier gas flow rate and chamber pressure and by the mixed effect of chamber pressure and carrier gas flow rate.

The results obtained from this experimental spray program indicate that the RF plasma system can be successfully used for the complete melting and thus successful deposition of tungsten powders of the commercially available particle sizes. Also, the present research has commenced and progressed the establishment of the link between the integral properties of the spray plume and the resultant deposit properties.

Acknowledgments

The financial support of the Natural Sciences and Engineering Research Council of Canada (NSERC) and the Ministry of Education of the Province of Québec through its (FQRNT) programme are gratefully acknowledged. This project was also partially funded and supported by Tekna Plasma Systems Inc. in Sherbrooke, Québec. O. Kovářík acknowledges the financial support from Czech Science Foundation project No.106/05/0483.

References

1. M. El-Hage, J. Mostaghimi, and M.I. Boulos, A Turbulent Flow Model for the RF Inductively Coupled Plasma, *J. Appl. Phys.*, 1996, **65**(11), p 4178-4185
2. J. Mostaghimi and M.I. Boulos, Effect of Frequency on Local Thermodynamic-Equilibrium Conditions in an Inductively Coupled Argon Plasma at Atmospheric-Pressure, *J. Appl. Phys*, 1990, **68**(6), p 2643-2648
3. S. Dresvin, K. Nguyen, D. Ivanov, and J. Amouroux, Calculation of RF Plasma Torch Parameters by Means of Non-Equilibrium Model, of AR Plasma, *High Temp. Mater. Process.*, 2001, **5**(1), p 93-98
4. S.W. Xue, P. Proulx, and M.I. Boulos, Extended-Field Electromagnetic Model for Inductively Coupled Plasma, *J. Phys. D: Appl. Phys.*, 2001, **34**(12), p 1897-1906
5. M. Rahmane, G. Soucy, and M.I. Boulos, Diffusion Phenomena of a Cold Gas in a Thermal Plasma Stream, *Plasma Chem. Plasma Process.*, 1996, **16**(1), p 169-189
6. M. Boulos, Heating of Powders in the Fire Ball of Induction Plasma, *IEEE Trans. Plasma Sci.*, 1978, **PS-6**(2), p 93-105
7. P. Proulx, J. Mostaghimi, and M.I. Boulos, Heating of Powders in an RF Inductively Coupled Plasma Under Dense Loading Conditions, *Plasma Chem. Plasma Process.*, 1987, **7**(1), p 29-52
8. R. Ye, P. Proulx, and M.I. Boulos, Particle Turbulent Dispersion and Loading Effects in an Inductively Coupled Radio Frequency Plasma, *J. Phys. D: Appl. Phys.*, 2000, **33**(17), p 2154-2162
9. M. Shigeta, T. Sato, and H. Nishiyama, Computational Simulation of a Particle-Laden RF Inductively Coupled Plasma with Seeded Potassium, *Int. J. Heat Mass Transfer*, 2004, **47**(4), p 707-716
10. K. Remesh, S.C.M. Yu, C.C. Berndt, Computational Study and Experimental Comparison of the In-Flight Particle Behavior for an External Injection Plasma Spray Process, J. Therm. Spray Technol., 12(4), 508–522
11. H.B. Xiong, L.L. Zheng, M.Y. Zhang, H. Zhang, J. Margolies, and S. Sampath, Numerical Study of Particle In-Flight Characteristics in a RF Induction Plasma Spray, in *Thermal Spray Connects: Explore its Surfacing Potential*, E. Lugscheider, Ed., May 2-4, 2005 (Basel, Switzerland), ASM International, 2005
12. S. Coulombe, M.I. Boulos, and T. Sakuta, Simultaneous Particle Surface-Temperature and Velocity-Measurements Under Plasma Conditions, *Meas. Sci. Technol.*, 1995, **6**(4), p 383-390
13. Z. Salhi, S. Guessasma, P. Gougeon, D. Klein, and C. Coddet, Diagnostic of YSZ In-Flight Particle Characteristics Under Low Pressure VPS Conditions, *Aerospace Sci. Technol.*, 2005, **9**(3), p 203-209
14. A. Kucuk, R.S. Lima, and C.C. Berndt, Influence of Plasma Spray Parameters on In-Flight Characteristics of ZrO2-8 wt% Y2O3 Ceramic Particles, *J. Am. Ceram. Soc.*, 2001, **84**(4), p 685-692
15. J. Vattulainen, E. Hämäläinen, R. Hernberg, P. Vuoristo, and T. Mäntylä, Novel Method for In-Flight Particle Temperature and Velocity Measurements in Plasma Spraying Using a Single CCD Camera, *J. Therm. Spray Technol.*, 2001, **10**(1), p 94-104
16. M. Vardelle, A. Vardelle, P. Fauchais, and M.I. Boulos, Plasma-Particle Momentum and Heat-Transfer – Modeling and Measurements, *AICHE J*, 1983, **29**(2), p 236-243
17. S. Das, V.K. Suri, U. Chandra, and K. Sampath, One-Dimensional Mathematical-Model for Selecting Plasma Spray Process Parameters, *J. Therm. Spray Technol.*, 1995, **4**(2), p 153-162
18. J. Tinoco, B. Widell, H. Fredriksson, and L. Fuchs, Modeling the In-Flight Events During Metal Spray Forming, *Mater. Sci. Eng. A*, 2004, **365**(1-2), p 302-310
19. M.P. Planche, R. Bolot, and C. Coddet, In-flight Characteristics of Plasma Sprayed Alumina Particles: Measurements, Modeling, and Comparison, *J. Therm. Spray Technol.*, 2003, **12**(1), p 101-111
20. O. Kovarik, S. Xue, X. Fan, and M.I. Boulos, RF Plasma Deposition of Refractory Metals, Case Study for Tungsten, *Thermal Spray: Building on 100 Years of Success*, E. Lugscheider, Ed., May 15-18, 2006 (Seattle, WA), ASM International, 2006
21. X.L. Jiang, M.I. Boulos, Particle Melting, Flattening, and Stacking Behaviors in Induction Plasma Deposition of Tungsten, Trans. Nonferr. Metal. Soc., 11(6), 811–816
22. X.L. Jiang, R. Tiwari, F. Gitzhofer, and M.I. Boulos, On the Induction Plasma Deposition of Tungsten Metal, *J. Therm. Spray Technol.*, 1993, **2**(3), p 265-270
23. X. Fan and M.I. Boulos, Near-Net Shape Forming of Tungsten Material by Induction Plasma Deposition, *Thermal Spray Connects: Explore its Surfacing Potential*, E. Lugscheider, Ed. , May 2-4, 2005 (Basel, Switzerland), ASM International, 2005, p 405-408
24. M. Krauss, D. Bergmann, U. Fritsching, and K. Bauckhage, In-situ Particle Temperature, Velocity and Size Measurements in the Spray Forming Process, *Mater. Sci. Eng. A*, 2002, **326**(1), p 154-164
25. P.S. Grant, B. Cantor, and L. Katgerman, Modeling of Droplet Dynamic and Thermal Histories During Spray Forming, 1. Individual Droplet Behavior, *Acta Metall. Mater.*, 1993, **41**(11), p 3097-3108
26. P. Buchner, H. Schubert, J. Uhlenbusch, and M. Weiss, Diagnostics of an RF Plasma Flash Evaporation Process Using the Monochromatic Imaging Technique, *Plasma Chem. Plasma Process.*, 2001, **21**(1), p 1-21
27. X.L. Jiang and M. Boulos, Induction Plasma Spheroidization of Tungsten and Molybdenum Powders, *Trans. Nonferr. Met. Soc. China*, 2006, **16**(1), p 13-17
28. G.E.P. Box, W.G. Hunter, and J.S. Hunter, *Statistics for Experimenters: An Introduction to Design, Data Analysis, and Model Building*, John Wiley and Sons, 1978